AD-A272 922

Estimating the Rotation Rate of Mesoscale Ocean Rings from Satellite Altimetry

THEODORE J. BENNETT, JR.

Ocean Dynamics and Prediction Branch
Oceanography Division

DTIC
ELECTE
NOV 19 1993
B

October 26, 1993

93-28102

REPORT DOCUMENTATION PAGE

Public reporting burden for this collection of information is estimated to average 1 hour per response, including the time for reviewing instructions, searching existing data sources, gathering and maintaining the data needed, and completing and reviewing the collection of information. Send comments regarding this burden or any other aspect of this collection of information, including suggestions for reducing this burden, to Washington Headquarters Services, Directorate for information Operations and Reports, 1215 Jefferson Davis Highway, Suite 1204, Arlington, VA 22202-4302, and to the Office of Management and Budget, Paperwork Reduction Project (0704-0188), Washington, DC 20503

1. AGENCY USE ONLY *(Leave blank)*	2. REPORT DATE October 26, 1993	3. REPORT TYPE AND DATES COVERED Final

4. TITLE AND SUBTITLE

Estimating the Rotation Rate of Mesoscale Ocean Rings from Satellite Altimetry

6. AUTHOR(S)

Theodore J. Bennett, Jr.*

5. FUNDING NUMBERS

Job Order No   93221K

Program Element No   0603207N

Project No   X2008

Task No

Accession No   DN258048
                      DN259001

7. PERFORMING ORGANIZATION NAME(S) AND ADDRESS(ES)

Naval Research Laboratory
Oceanography Division
Stennis Space Center, MS 39529-5004

8. PERFORMING ORGANIZATION REPORT NUMBER

NRL/FR/7322--93-9443

9. SPONSORING/MONITORING AGENCY NAME(S) AND ADDRESS(ES)

Space and Naval Warfare Systems Command
PDW-106-8
Washington, DC 20361

10. SPONSORING/MONITORING AGENCY REPORT NUMBER

11. SUPPLEMENTARY NOTES

*Now at the Naval Oceanographic Office, Stennis Space Center, MS 39522-5001.

12a. DISTRIBUTION/AVAILABILITY STATEMENT

Approved for public release; distribution unlimited.

12b. DISTRIBUTION CODE

13. ABSTRACT *(Maximum 200 words)*

The mesoscale ocean environment has considerable impact on underwater acoustics. However, the ocean is such a data-sparse environment, especially at depth, that it is difficult to make effective ocean nowcasts and forecasts of the environment. A key input to nowcasts and forecasts is the rotation rate of mesoscale ocean rings. This report presents a technique for determining the rotation rate from satellite altimetry. The technique offers the prospect of a cost-effective system for monitoring this key ocean parameter.

14. SUBJECT TERMS	15. NUMBER OF PAGES 18
tactical scale models, ocean models, data assimilation	
	16. PRICE CODE

17. SECURITY CLASSIFICATION OF REPORT	18. SECURITY CLASSIFICATION OF THIS PAGE	19. SECURITY CLASSIFICATION OF ABSTRACT	20. LIMITATION OF ABSTRACT
Unclassified	Unclassified	Unclassified	Same as report

CONTENTS

ESTIMATING THE ROTATION RATE OF MESOSCALE OCEAN RINGS FROM SATELLITE ALTIMETRY

INTRODUCTION

The U.S. Navy's thermal analysis system assimilates data into a three-dimensional depiction of the ocean thermal structure. The input data for the analysis includes bathythermographs, ship and buoy temperatures, and satellite-derived sea surface temperatures. In addition, a key input to the system is a map of the surface locations of fronts and rings, together with estimates of such parameters as the ring rotation rate. This map is assimilated into the analysis via feature models. A feature model is a schematic, diagnostic model that depicts the typical three-dimensional thermal structure of fronts and rings, and is used to infer the subsurface thermal structure from the surface location of fronts and rings. It is a powerful tool for supplementing sparse data with a knowledge of the oceanography of mesoscale ocean features.

Ring parameters are used to tune the ring feature model to agree with the characteristics of a particular ring. Experience has shown that the ring rotation rate is a key parameter for tuning the ring feature model. This report presents a technique for using satellite altimetry data to estimate the ring rotation rate. The technique is applicable even if the altimeter track does not cross the ring center. Applicability to tracks that do not cross the ring center is important because the study of Tournadre (1990) suggests a less than 5% probability that a given ring's center will lie on a GEOSAT or TOPEX/POSEIDON altimeter ground track. He also considers the case of an altimeter crossing within half a radius of the ring center. The percentage of Gulf Stream rings that have a probability greater than 50% of being detected (distance between the ring center and altimeter track is less than half a ring radius) is greater than 83% for the warm-core rings and 45% for the cold-core rings.

Section 2 presents some background on thermal analyses, front and ring maps, and feature models. The technique for estimating the ring rotation rate is discussed in Sec. 3. Examples of the application of this approach are presented in Sec. 4. Section 5 discusses how well the estimates agree with rates that have been reported in the literature, as well as the potential for assimilating drifting buoy data into a composite estimate. Conclusions are set forth in Sec. 6, and Sec. 7 has recommendations for future work.

BACKGROUND

Two key aspects of monitoring the ocean thermal structure are data and a thermal analysis system. The data are from disparate sources irregularly sampled in space and time, each with its own characteristic quality. The thermal analysis system assimilates these data into a regularly gridded map of the ocean thermal structure.

The U.S. Navy uses optimum-interpolation-based (Gandin 1965; Bretherton et al. 1976; White and Bernstein 1979) thermal analysis systems for making three-dimensional analyses of the ocean thermal structure. One system is known as the Optimum Thermal Interpolation System (OTIS) (Clancy 1987; Clancy et al. 1990). This system assimilates bathythermograph (BT) data, front and eddy maps, and sea surface temperature (SST) data from satellites, ships, and buoys. In addition, an OTIS analysis is used to initialize a forecast of the upper (400 m) ocean thermal structure by the Thermodynamic Ocean Prediction System (TOPS) (Clancy and Pollak 1983). The thermal analysis can also be used to initialize a dynamical ocean forecast model (Robinson and Walstad 1987; Fox et al. 1993). OTIS is presently operational in some regions at the Navy's Fleet Numerical Ocean-ography Center (FNOC). The Modular Ocean Data Assimilation System (MODAS) is a more modular and user-friendly version of OTIS that was developed at the Naval Research Laboratory. MODAS is being implemented in several areas for use at the Naval Oceanographic Office (NAVOCEANO).

A major impediment to the effective use of any thermal analysis system is the sparsity of data available for monitoring the mesoscale ocean, especially at depth. The BT is the principal source of subsurface temperature data, but there are only about 200 BTs per day for the world's oceans (Clancy 1987). SST data are obtained from ships and buoys. Although ship and buoy SST data are more abundant than BT data, ship data have larger errors. Satellite data offer the prospect of a cost-effective system for the long-term monitoring of the ocean environment (Hawkins et al. 1989). Satellite-derived SSTs have been used routinely for a number of years by the U.S. Navy as data for OTIS. These data are unobtainable, however, in cloud-covered areas.

More recently, mesocale fronts and rings have been located using satellite altimeter data (Lybanon et al. 1990; Cheney and Marsh 1981). Altimeter data are particularly useful for locating submerged cold-core rings that have no SST signature (Lybanon et al. 1990). However, the width of the altimetric footprint is very narrow. When the satellite is in an exact repeat mode, the ensemble of groundtracks form a grid that is periodically repeated. The spacing between the tracks can be reduced only at the expense of increasing the time between repetitions of the tracks. In the case of the GEOSAT Exact Repeat Mission, which was optimized for oceanographic applications, the grid has a spacing of 1.4754 degrees at the equator and a 17-day repeat cycle (Born et al. 1987). Hence, several days can elapse before a ring is revisited by the altimeter.

An important input to OTIS is a map, known as the bogus, of the surface location of mesoscale ocean fronts and rings. This map, together with estimates of various ring parameters and front characteristics, is produced by NAVOCEANO. The bogus is produced primarily by examining the thermal gradients found in satellite SST data. In addition, limited amounts of altimetry, BT, and other data are sometimes used. These data are sometimes adequate for mapping the front at the surface, but there are rarely enough subsurface data for mapping the three-dimensional thermal structure. The surface information in the bogus message is assimilated into the thermal analysis at depth by means of feature models (Robinson and Walstad 1987; Bennett et al. 1989).

The ring feature model of Bennett et al. (1989) is an example of a feature model that can be tuned using ring parameters. This model initially uses a typical ring rotation rate, the observed ring radius from the bogus, and simple dynamical arguments to estimate the field of dynamic height anomaly of the ring. The thermal structure of the ring can then be modeled by inferring from the dynamic height anomaly a temperature profile at each point on a close-mesh grid centered on the ring. The inferred profiles are often referred to as synthetic profiles. Bennett et al. (1989) used an iterative procedure to infer the synthetic profile. An alternative approach for inferring synthetic profiles of temperature, salinity, and sound speed has been evaluated by Carnes et al. (1990). They derived the empirical orthogonal functions (EOFs) of the variability of temperature and salinity

profiles from a domain of the ocean, and then determined a regression between the dynamic height anomaly and the amplitude of the EOFs. It is then straightforward to infer the EOF amplitudes from an estimate of dynamic height anomaly and to construct a synthetic profile.

Experience has shown that the ring rotation rate is a key parameter for tuning the ring feature model. For example, consider a cold-core ring that is described by the conceptual model presented in Joyce (1984) and Olson (1980) and discussed below. Assume the radius of the ring core is 75 km and the dynamic height anomaly at the edge of the core is 1.5 m, which is approximately that of the ambient water. For rotation rates of $2.0*10^{-5}$ s^{-1} and $2.5*10^{-5}$ s^{-1}, which is the approximate range of measured rates for cold-core rings, the dynamic height anomaly at the ring center is estimated via Eqs. (1) and (2) (presented below) to be 0.907 m and 0.723 m, respectively. The dynamic height anomaly and, hence, the subsurface thermal structure are seen to be sensitive to the rotation rate.

Glenn et al. (1990) describe techniques for estimating several ring parameters, including the rotation rate, by fitting feature models to satellite SST data, BT data, and drifting buoy data. They found that a feature model analysis of drifting buoy data is an effective means for monitoring the evolution of Gulf Stream rings. In addition, they used these techniques to provide real-time support for deep-water drilling operations off the East Coast of the U.S.

A number of techniques exist for assimilating the information in the bogus into an analysis via feature models. In the implementation known as OTIS 1.1 (Bennett et al. 1989), the bogus and feature models are used to construct the first-guess field, which resembles a climatology but has typical frontal and ring thermal structures built into it at the locations indicated in the bogus. The BT and SST data are then assimilated via optimum interpolation into this first-guess field. In data-sparse areas, the analysis will resemble the first-guess field, which has schematic descriptions of mesoscale features at the appropriate locations. In the OTIS 3.0 implementation, the first-guess field is a climatology. The feature model is then expressed as a number of synthetic profiles of temperature that are assimilated along with BT and other data into the climatology via optimum interpolation.

APPROACH

This report presents a technique for estimating the radius and rotation rate of a ring from a track of altimetry data. The technique is applicable even if the track does not cross the center of the ring. In addition, it is shown how to composite estimates from several such tracks into a best estimate of these ring parameters.

Consider a circular ring. Observations of warm-core (Joyce 1984) and cold-core (Olson 1980) rings indicate that near the surface a ring consists of a disk in solid body rotation surrounded by a transition zone within which the azimuthal velocity rapidly decreases to zero. The azimuthal velocity, v, satisfies the equation

$$fv + \frac{v^2}{r} = \frac{\partial \Phi}{\partial r} = g \frac{\partial z}{\partial r} \tag{1}$$

where f is the Coriolis parameter, r is the radial distance, and Φ is the geopotential anomaly between the sea surface and a reference level. The height (dynamic topography) associated with the geopotential anomaly is $z = \Phi/g$, where g is the acceleration of gravity. Substituting the condition of solid body rotation, $v = wr$, where w is the rotation rate of the ring, into Eq. (1) and integrating from the center of the ring outward gives

$$z = z_0 + \frac{w(w + f)}{2g} r^2 .$$ (2)

Consider a track of altimeter-derived dynamic topography data that crosses a disk of radius R and comes within a distance L of the ring center (see Fig. 1). In this report, z is used to represent the dynamic topography. Denote the minimum (maximum) dynamic topography z along the track as it crosses the ring as an origin and let l be the distance along the track from this origin. Beginning with Eq. (2), the dynamic topography along the track can be expressed as

$$z = z_0 + \frac{w(w + f)}{2g} L^2 + \frac{w(w + f)}{2g} l^2$$ (3)

or, more concisely, as

$$z = z_0' + c\, l^2 ,$$ (3a)

where

$$z_0' = z_0 + \frac{w(w + f)}{2g} L^2$$ (3b)

and

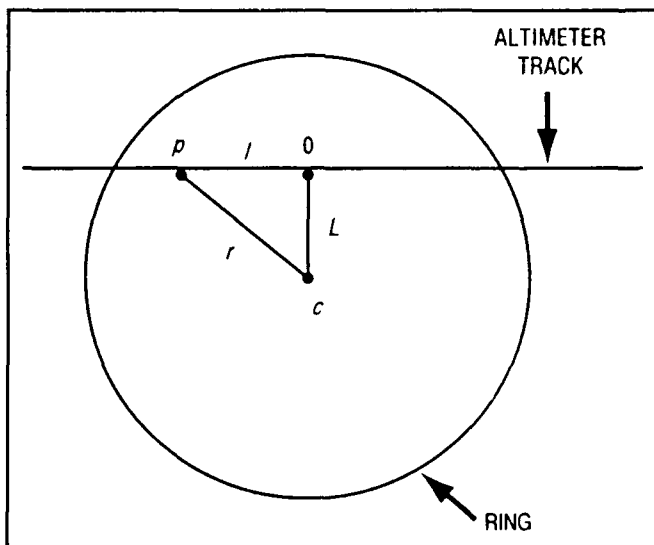$$c = \frac{w(w + f)}{2g} .$$ (3c)

Fig. 1 — The ground track of the satellite altimeter crosses a ring at a distance L from the center c of the ring. The dynamic topography of a cold-core (warm-core) ring has a minimum (maximum) along the track at location 0, which is labeled the origin in this context. The point p along the track is a distance l from point 0 and a distance r from the ring center at c. Note $r = (l^2 + L^2)^{1/2}$.

The parameter z_0' is an estimate of the minimum (maximum) dynamic topography along the track as the altimeter crosses the cold-core (warm-core) ring. The curvature (rate of change of slope) of the dynamic topography is 2*c.

The application of the approach begins by estimating the dynamic topography along the altimeter track. The location of the origin (the dynamic topography minimum or maximum along the track as it crosses the ring) is then determined by inspection and the dynamic topography is plotted as a function of distance l from the origin. Least squares are used to determine the quadratic equation, Eq. (3a), that best fits the dynamic topography as a function of l. The rate of rotation w is then readily estimated from c and the known latitude via

$$w = \frac{-f \pm \sqrt{(f^2 + 2gc)}}{2} .$$ (4)

The positive (negative) root is used in Eq. (4) for cold (warm) rings. Note that the estimate of the ring rotation rate does not depend on the distance from the track to the ring center as long as the track crosses the core that is in solid body rotation.

The rotation rates estimated from several tracks of altimetry data can be readily assimilated into a composite estimate. Consider, for example, repeated passes of the altimeter along a particular ground track as a cold-core ring drifts across the ground track. The composite w can be estimated by averaging those estimated values of w that pass a gross error check. The uncertainty in the composite w can be estimated from the variabili$w$ of the w estimates within the albeit quite limited distribution. In addition, the minimum z_0' that passes a gross error check is the best estimate of z at the center of the cold-core ring.

RESULTS

Rotation Rate from a Single Altimeter Track

In this section, we estimate the rotation rate of a cold-core ring from a single track of altimetry data. Figure 2 is a plot of the dynamic topography along the ascending ground track A4 of the GEOSAT Exact Repeat Mission. The technique for estimating dynamic topography is a modification of the approach of Carnes (private communication) and is summarized in the appendix. These data are from revolution 11311 of the GEOSAT altimeter, which occurred on 12 May 1987. The location
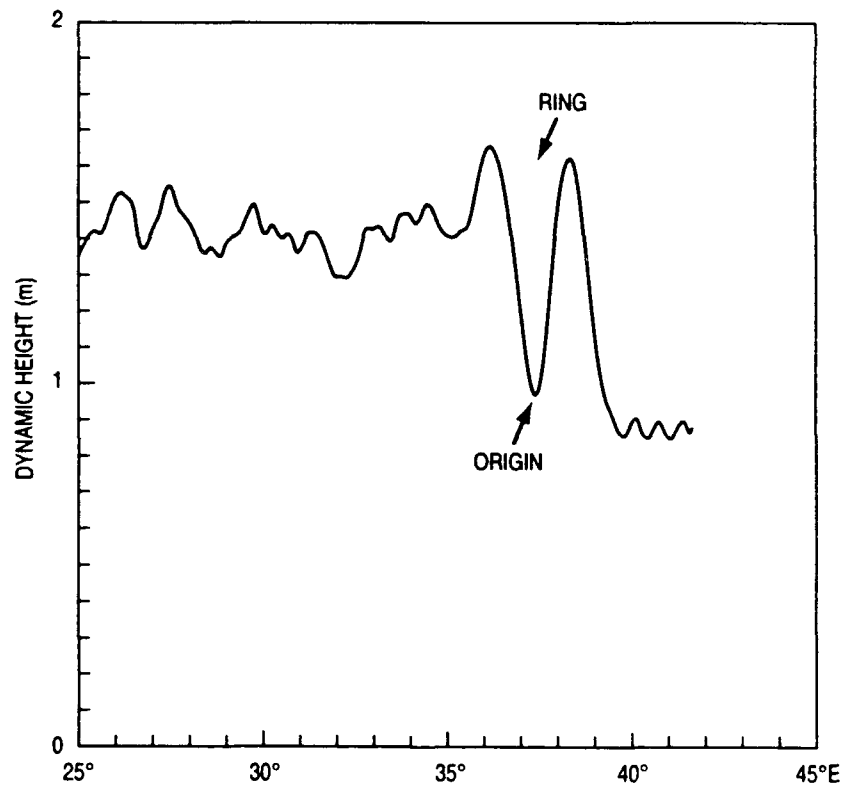

Fig. 2 — The dynamic topography along ground track A4 for revolution 11311 of the GEOSAT altimeter. A cold-core ring is located near 37° N–38° N. The location of the minimum dynamic topography is the origin.

of a cold-core ring and the choice of the origin are also indicated on Fig. 2. By comparing this track of dynamic topography to neighboring tracks and by examining the time evolution of the tracks, the interpretation of the data in Fig. 2 as a front and cold-core ring rather than as a front and a warm-core ring can be made.

Figure 3 is a plot of all dynamic topography estimates that lie within 125 km of the origin. The "+" signs represent data from points that lie south of the origin, and the "*" signs represent data from points to the north. A least-squares quadratic fit of all of the data that lie within a distance s of the origin is made for several values of s. The resulting curves are shown in Fig. 4. The data that lie within about 75 km of the origin fit a quadratic curve rather well; a disk in solid body rotation describes these data well. Between 75 and 125 km, there is the transition zone within which the azimuthal velocity decreases to zero with increasing distance from the origin. The dynamic topography and fitted curve diverge with increasing distance within the transition zone. The dynamic topography at a distance of 125 km is approaching that of the ambient water.

Table 1 presents, for several values of s, the coefficient of determination (Mack 1966) and standard deviation of the data about the fitted quadratic. The coefficient of determination is the ratio of the variance explained by the curve to the total variance. The coefficient is close to 1.0, indicating that the curve fits the data well as can be seen by inspection. The standard deviation of the data about the fitted curve is only on the order of a few centimeters. The data are from a crossing of a cold-core ring by the GEOSAT altimeter during revolution 11311.
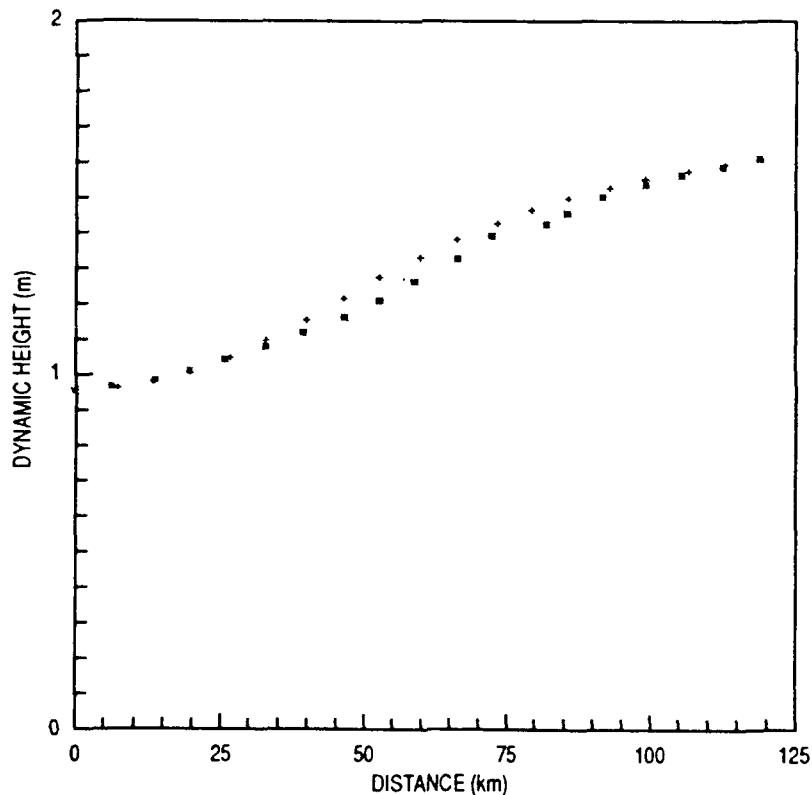

Fig. 3 — A plot of dynamic topography (from Fig. 2) as a function of distance from the origin. The + symbols signify points south of the origin and the * symbols signify points north.
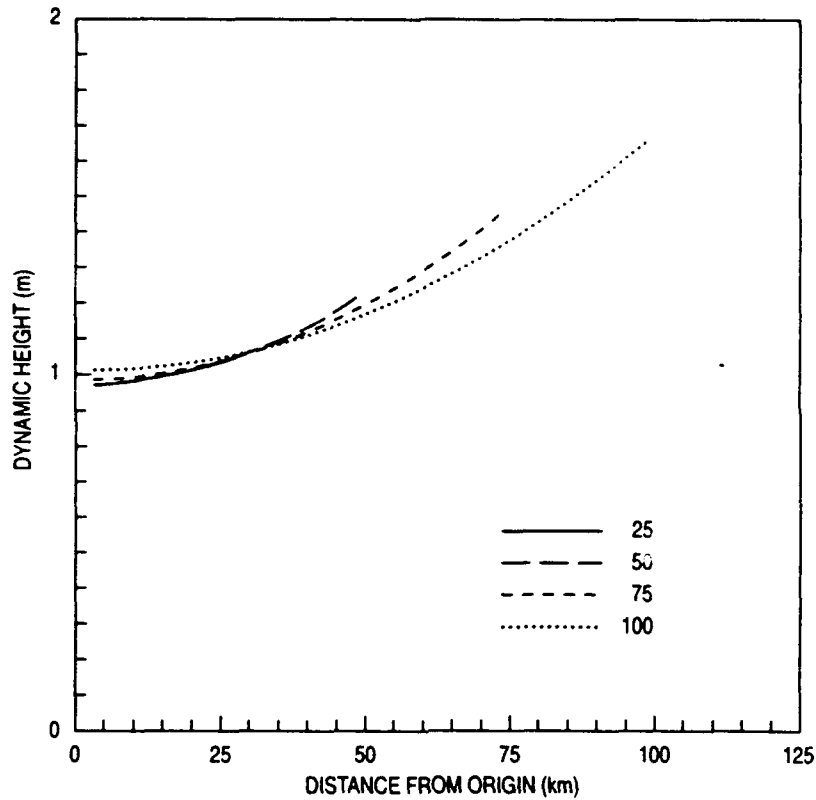
Fig. 4 — Quadratic curves fitted in a least-squares sense to the dynamic topography vs. distance data of Fig. 3. Separate fits are made of data that is within 25, 50, 75, and 100 km of the origin.

Table 1 — The Coefficient of Determination and the Standard Deviation of the Dynamic Topography vs. Distance Data About the Fitted Curve

s (km)	25	50	75	100
Coefficient of Determination	0.98	0.95	0.95	0.91
Standard Deviation (cm)	0.18	1.3	2.8	5.5

As the data to be fitted are restricted to lie closer to the origin, the curvature of the fitted curve increases. Table 2 presents the parameters z_0' and c, as well as the rotation rate w for each of the curves fitted to the data and shown in Fig. 4. The estimated w is $1.7*10^{-5}$ s^{-1} when a fit is made to all of the data that lie within 75 km of the origin. If the origin were to lie at the center of the ring, then the ring radius would be about 75 km. The data are from a crossing of a cold-core ring by the GEOSAT altimeter during revolution 11311.

Repeated Altimeter Tracks

In this section we consider the case of repeated passes of the satellite altimeter along a single ground track as a cold-core ring drifts across the ground track. Figure 5 presents the dynamic

Table 2 — Parameters z_0' and c and the Estimated Ring Rotation Rate w for Several Least-Squares Quadratic $\left(z_0' + c\,l^2\right)$ Fits of the Dynamic Topography vs. Distance Data

s (km)	z_0' (m)	c $(10^{-4}$m km$^{-2})$	w $(10^{-5}$ s$^{-1})$
25	1.0	1 247	2.3
50	1.0	i.055	2.0
75	1.0	0.870	1.7
100	1.0	0.666	1.3

topography for revolutions 10823, 11067, and 11311 along the GEOSAT ascending ground track A4. The tracks of dynamic topography are offset by 0.2 m for clarity. These tracks are 17 days apart and are dated 8 April 1987, 25 April 1987, and 12 May 1987. The data for revolution 11311 were considered in Sec. 4.1.

Figures 6 and 7 are plots of the dynamic topography vs. distance from the origin for tracks 10823 and 11067, respectively. Also shown on each figure is the quadratic curve fitted in a least-squares sense to all the data that lie within 75 km of the origin. The curve is shown for the case of fitting all data within 75 km of the origin because the coefficient of determination is larger at $s = 75$ km than at $s = 25$, 50, or 100 km, although the difference was minimal for revolution 10823. In the case of track 11067, the data from north and south of the origin did not agree with each other as well as did similar comparisons from the other two tracks. The dynamic topography at the origin is about 0.18 m higher in the case of track 10823 than track 11067, suggesting that the track of altimetry data crosses the ring at a longer distance from the ring center in the case of track 10823. Both tracks
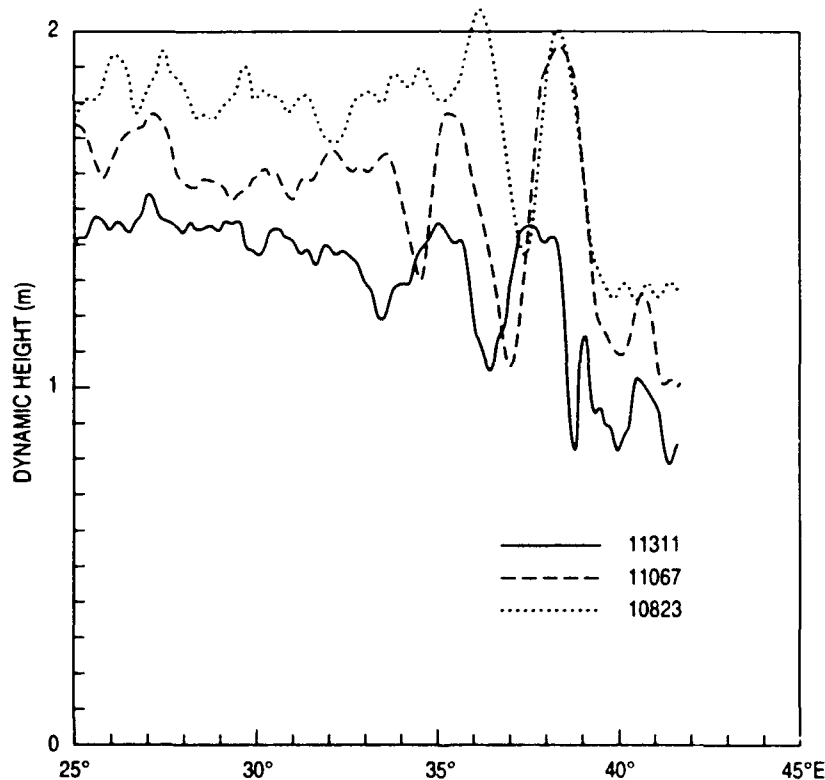

Fig. 5 — The dynamic topography along ground track A4 for revolutions 10823, 11067, and 11311 of the GEOSAT altimeter. The tracks are offset by 0.2 m for clarity. These revolutions are consecutive passes along track A4 during the GEOSAT Exact Repeat Mission. (Note the cold-core ring drifting across the track near 36° N–38° N)
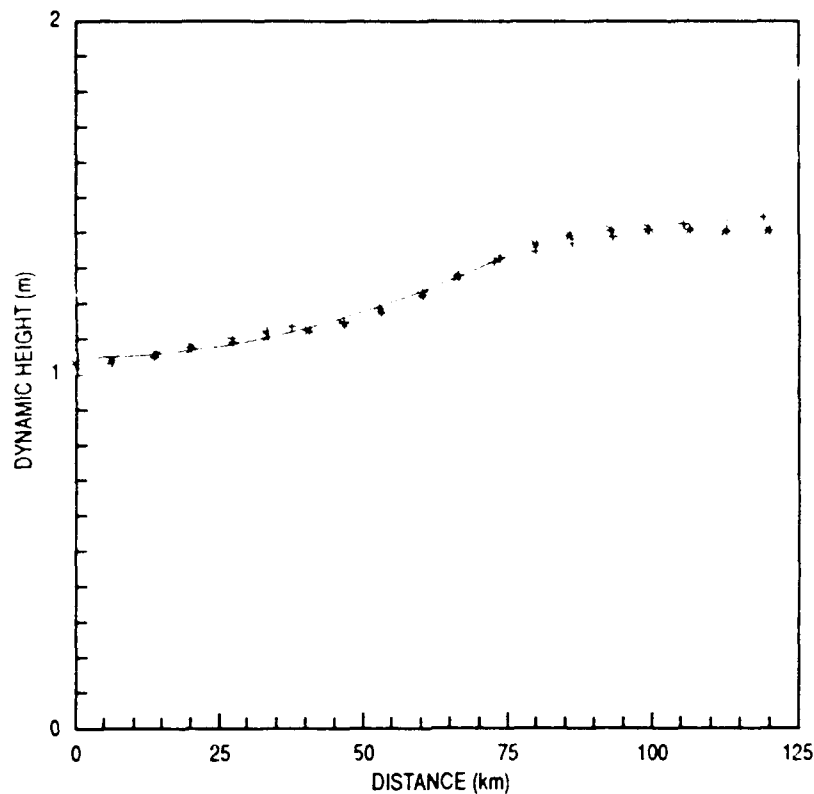
Fig 6 — A plot of dynamic topography from GEOSAT revolution 10823 as a function of distance from the origin. The + symbols signify points south of the origin and the * symbols signify points north. Also shown is a least-squares quadratic fit of the data that lie within 75 km of the origin.

10823 and 11067 have a "bump" in the dynamic topography relative to the quadratic curve at distances of 30–40 km.

The ring rotation rates estimated from these curves are tabulated in Table 3. The parameters are obtained by making a least-squares quadratic $\left(z'_0 + c\,l^2\right)$ fit of the dynamic topography vs. distance data. Each fit is made of the data that lie within 75 km of the origin. Composite 1 is a composite of all three tracks while composite 2 is a composite of tracks 11067 and 11311 only. A value of $s = 75$ km is also used for revolution 11311. The coefficient of determination for this case (0.95) was comparable to, although smaller, than the largest value (0.98). However, the subjective judgment was made that a value of s that is long and representative of the range of distances over which the conceptual model is considered valid, is better than a very short value of s. These data suggest that a single track of altimetry is insufficient for making a confident estimate of the ring rotation rate. The rates estimated from tracks 11067 and 11311 agree rather well with each other but the rate determined from track 10823 is only 60% of that from track 11311.

The most confident estimate of the ring parameters is obtained by compositing estimates from several tracks. The composite w is the average of all of the values that pass a gross error check. In this case, the estimates of w from tracks 11067 and 11311 agree well with each other, but the estimate from track 10823 is somewhat of an outlying estimate. All three tracks are included in composite 1 to give a composite w of $1.4*10^{-5}$ s^{-1}. If only tracks 11067 and 11311 were included (composite 2), then the composite rotation rate is $1.6*10^{-5}$ s^{-1}. In addition, all three values of z'_0
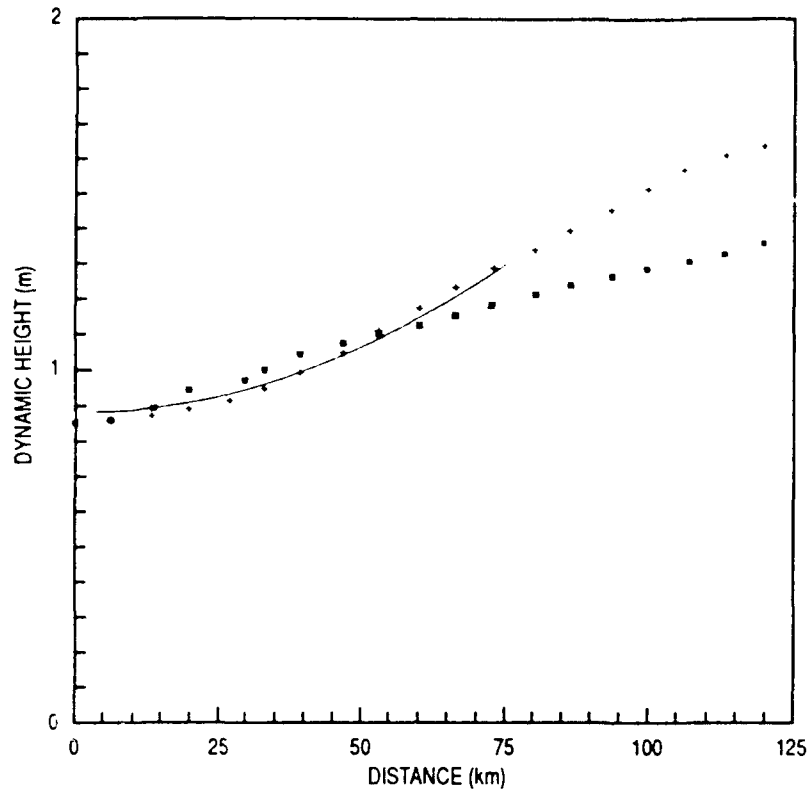
Fig. 7 — A plot of dynamic topography from GEOSAT revolution 11067 as a function of distance from the origin. The + symbols signify points south of the origin and the * symbols signify points north. Also shown is a least-squares quadratic fit of the data that lie within 75 km of the origin.

Table 3 — Parameters z_0' and c and the Estimated Ring Rotation Rate w for Each of Three Tracks of GEOSAT Altimetry Data that Crosses a Particular Cold-Core Ring

Rev.	z_0' (m)	c (10^{-4}m km^{-2})	w (10^{-5} s^{-1})
10823	1.1	0.489	1.0
11067	0.9	0.766	1.5
11311	1.0	0.870	1.7
Composite 1	0.9		1.4
Composite 2	0.9		1.6

are plausible and the minimum value, 0.9 m, is chosen as the best estimate of the dynamic topography at the center of the ring.

As the ring drifts past track A4 and across track A3, estimates of the rotation rate obtained using the data from along track A3 can also be assimilated into the composite estimate of the rotation rate. If the ring were large enough to extend across two neighboring tracks, then estimates obtained from both tracks could be used in the composite.

DISCUSSION

While there are no concurrent altimeter and ring rotation rate data to verify these estimates of the ring rotation rate, these estimates can be compared to the measured rotation rates of other rings. The comparison shows that these estimates are realistic but perhaps a little slow. Vastano et al. (1980) gives the azimuthal speed of cold-core ring Bob (Olson 1980) as 2.26 km h^{-1} at a radius of 30 km, which gives a rotation rate of $2.1*10^{-5}$ s^{-1}. Richardson (1983) has reviewed Gulf Stream rings, including their rotation rates. He states that young rings have surface swirl velocities of about 1.5 m s^{-1} at a distance of 30–60 km from the ring center. The corresponding rotation rate is $2.5*10^{-5}$ s^{-1} to $5.0*10^{-5}$ s^{-1}. Flierl (1979) describes a simple model of warm- and cold-core rings. His model assumes an inviscid, uniformly rotating two-layer fluid. The lower layer is at rest and the upper layer has constant potential vorticity. Using the Flierl model (Flierl 1979, Fig. 10) gives an estimated rotation rate of $2.4*10^{-5}$ s^{-1} for a cold-core ring with a radius of 75 km.

Individual estimates of the rotation rate can differ for a number of reasons. The geoid could have errors in it. The ring could be elliptical rather than circular. The wet tropospheric (water vapor) correction to altimeter-derived ocean topography can be large enough to mimic or mask true ocean features (Phoebus and Hawkins 1990). Without an adequate estimate of this correction, consecutive altimeter-derived estimates of the dynamic topography of a ring could show significant variation due just to atmospheric water vapor. These data did not have a wet tropospheric correction. The rotation rate could also change over time. The decay time scale for available potential energy, kinetic energy, and total energy for an isolated Gulf Stream ring is on the order of 500 days. However, interactions with the bottom topography and the Gulf Stream can decrease the time scale by a factor of 10 (Olson et al. 1985). Hence, estimates of the ring rotation rate before and after such interactions can be quite different.

Estimates of the ring rotation rate from other data sources can also be assimilated into the composite estimate. In particular, the spiral path of a drifting buoy that is imbedded in a ring can be used to infer the location of the ring center, the translation speed and direction, and the rate of rotation (see, for example, Armi et al. (1989) and Richardson et al. (1989)). A 30-day record of drifting buoy data could be subdivided into three 10-day records and a rotation rate estimated from each 10-day period. At least one complete ring rotation would likely occur within the 10-day period. The rotation period of a new ring is about 2 days and that for an aged, less energetic ring is about 5–10 days (Richardson 1983). The three estimates of ring rotation rate inferred from the altimeter could be averaged with the three estimates from the drifting buoy data. The relative weights of the two types of estimates could be determined from the relative spread of the individual estimates about the average for their data type.

Satellite altimetry, satellite IR imagery, and drifting buoys could complement each other to become key elements of a cost-effective system for monitoring ocean rings, especially submerged cold rings that have no surface signature. The altimeter data could be used to determine that a ring exists in an area and, using the present technique, estimate its rotation rate. However, the distance of the altimeter track from the ring center is unknown, and it is not known on which side of the altimetry track the ring center lies. Satellite IR imagery could be used in some cases to locate the ring center, to estimate the ring radius, and to determine how far from and on which side of the track the ring center lies. A drifting buoy can be used to locate the ring center and estimate the rotation rate for a period of up to several months, including those periods when the ring lies between the altimetry tracks. However, drifting buoys are an inefficient means to initially locate rings. Used together, data from altimetry and drifting buoys can overcome these shortcomings. The altimeter data could be used to target the deployment of the buoys. Both altimetry and drifting buoy data could be used to estimate the ring rotation rate. Finally, data from the drifting buoy could be

used to locate the center of the ring. The location of the ring center and the ring rotation rate and radius are the key inputs for a feature model description of the ring.

CONCLUSIONS

This report presented a technique for estimating the rotation rate of a mesoscale ocean ring from satellite altimetry. The technique was applied to the case of repeated passes of the satellite altimeter as a cold-core ring drifts across the ground track. The following are conclusions of the work:

(1) A least-squares quadratic curve fits the altimeter-estimated dynamic topography well within the core of the ring.

(2) A plausible estimate of the ring rotation rate can be readily obtained from the fitted quadratic curve.

(3) The most confident estimate of the rotation rate is obtained not from a single data track but from a composite of several tracks.

RECOMMENDATIONS

The following recommendations are made.

(1) Study the proposed technique for estimating the ring rotation rate more thoroughly by considering a number of cases for which the rotation rate is known from in situ data.

(2) Study and demonstrate a technique for assimilating rotation rate estimates from a satellite altimeter and a drifting buoy into a composite estimate.

ACKNOWLEDGMENTS

REFERENCES

Armi, L., D. Hebert, N. Oakley, J. F. Price, P. L. Richardson, H. T. Rossby, and B. Ruddick, "Two Years in the Life of a Mediterranean Salt Lens," *J. Phys. Oceanogr.* **19**, 354–370 (1989).

Bennett, Jr., T. J., M. R. Carnes, P. A. Phoebus, and L. M. Riedlinger, "Feature Modeling: The Incorporation of a Front and Eddy Map into Optimum Interpolation-Based Thermal Analyses," Naval Research Laboratory, Stennis Space Center, MS, NORDA Report 242, 1989.

Born, G. H., J. L. Mitchell, and G. A. Heyler, "Design of the GEOSAT Exact Repeat Mission," *Johns Hopkins APL Technical Digest* **8**, 260–266. (1987)

Bretherton, F. P., R. E. Davis, and C. B. Fandry, "A Technique for Objective Analysis and Design of Oceanographic Experiments Applied to MODE-O473," *Deep-Sea Res.* **23**, 559–582 (1976).

Carnes, M. R., J. L. Mitchell, and P. W. deWitt, "Synthetic Temperature Profiles Derived from GEOSAT Altimetry: Comparison with AXBT Profiles," *J. Geophys. Res.* **95**, 17979–17992 (1990).

Carnes, M. R., Naval Research Laboratory, Stennis Space Center, MS, private communication, 1991.

Cheney, R. E. and J. G. Marsh, "Seasat Altimeter Observations of Dynamic Topography in the Gulf Stream Region," *J. Geophys. Res.* **86**, 473–483 (1981).

Clancy, R. M., "Real-Time Applied Oceanography at the Navy's Global Center," *Marine Tech. Soc. J.* **21**, 33–46 (1987).

Clancy, R. M., P. A. Phoebus, and K. D. Pollak, "An Operational Global-Scale Ocean Thermal Analysis System," *J. Atmos. and Oceanic Tech.* **7**, 233–254 (1990).

Clancy, R. M. and K. D. Pollak, "A Real-Time Synoptic Ocean Thermal Analysis/Forecast System," *Prog. Oceanog.* **12**, 383–424 (1983).

Flierl, G. R., "A Simple Model for the Structure of Warm and Cold Core Rings," *J. Geophys. Res.* **84**, 781–785 (1979).

Fox, D. N., M. R. Carnes, and J. L. Mitchell, "Circulation Model Experiments of the Gulf Stream Using Satellite-Derived Fields," Naval Research Laboratory, Stennis Space Center, MS, NRL/FR/7323--92-9412, April 1993.

Gandin, L. S., "Objective Analysis of Meteorological Fields," *Israel Program for Scientific Translations* 242 pp., Jerusalem (1965).

Glenn, S. M., G. Z. Forristall, P. Cornillon, and G. Milkowski, "Observations of Gulf Stream Ring 83-E and Their Interpretation Using Feature Models," *J. Geophys. Res.* **95**, 13043–13063 (1990).

Glenn, S. M., D. L. Porter, and A. R. Robinson, "A Synthetic Geoid Validation of Geosat Mesoscale Dynamic Topography in the Gulf Stream Region," *J. Geophys. Res.* **96**, 7145–7166 (1991).

Hawkins, J., P. Phoebus, and D. May, "Remote Sensing Input to Navy Ocean Nowcasts/Forecasts," Proceedings of OCEANS '89, Seattle, WA, 1989, pp. 1004–1008.

Joyce, T. M., "Velocity and Hydrographic Structure of a Gulf Stream Warm-Core Ring," *J. Phys. Oceanogr.* **14**, 936–947 (1984).

Lybanon, M., R. L. Crout, C. H. Johnson, and P. Pistek, "Operational Altimeter-Derived Oceanographic Information," The NORDA GEOSAT Ocean Applications Program, *J. Atmos. and Oceanic Tech.* **7**, 357–376 (1990).

Mack, C., *Essentials of Statistics for Scientists and Technologists.* (Plenum Publishing Corporation, New York, NY, 1966).

Maul, G. A., J. R. Proni, M. Bushnell, and J. L. Mitchell, "Oceanic Dynamic Height Anomaly from GEOSAT: A Conceptual Model for Short Collinear Orbit Segments," *Marine Geodesy* **12**, 259–285 (1988).

Olson, D. B., "The Physical Oceanography of Two Rings Observed by the Cyclonic Ring Experiment. Part II: Dynamics," *J. Phys. Oceanogr.* **10**, 514–528 (1980).

Olson, D. B., R. W. Schmitt, M. Kennelly, and T. M. Joyce, "A Two-Layer Diagnostic Model of the Long-Term Physical Evolution of Warm-Core Ring 82B," *J. Geophys. Res.* **90**, 8813–8822 (1985).

Phoebus, P. A. and J. D. Hawkins, "The Impact of the Wet Tropospheric Correction on the Interpretation of Altimeter-Derived Ocean Topography in the Northeast Pacific," *J. Geophys. Res.* **95**, 2939–2952 (1990).

Richardson, P. L., "Gulf Stream Rings," in *Eddies in Marine Science*, A. R. Robinson, ed., (Springer-Verlag, Berlin and Heidelberg, 1983), p. 19–45.

Richardson, P. L., D. Walsh, L. Armi, M. Schroder, and J. F. Price, "Tracking Three Eddies with SOFAR Floats," *J. Phys. Oceanogr.* **19**, 371–383 (1989).

Robinson, A. R. and L. J. Walstad, "The Harvard Open Ocean Model: Calibration and Application to Dynamical Processes, Forecasting and Data Assimilation Studies," *Applied Numerical Mathematics* **3**, 89–131 (1987).

Tournadre, J., "Sampling of Oceanic Rings by Satellite Radar Altimeter," *J. Geophys. Res.* **95**, 693–697 (1990).

Vastano, A. C., J. E. Schmitz, and D. E. Hagan, "The Physical Oceanography of Two Rings Observed by the Cyclonic Ring Experiment. Part I: Physical Structures," *J. Phys. Oceanogr.* **10**, 493–513 (1980).

White, W. B. and R. L. Bernstein, "Design of an Oceanographic Network in the Midlatitude North Pacific," *J. Phys. Oceanogr.* **9**, 592–606 (1979).

APPENDIX

This appendix documents how the dynamic topography was obtained for use in this report. The terminology follows that of Maul et al. (1988).

The sea surface height ssh (the distance from the reference ellipsoid to the sea surface) is

$$ssh = z_s - z_a, \tag{A1}$$

where z_s is the height of the satellite above the reference ellipsoid as determined by tracking and z_a is the altimeter-derived estimate of the distance from the altimeter to the sea surface. It can be written as a sum

$$ssh = z_g + z_{BC} + z_{BT} + z_e, \tag{A2}$$

where z_g is the geoid, z_{BC} is the dynamic topography, z_{BT} is the barotropic part of the ssh, and z_e is a sum of various errors such as orbit error. From Eq. (A2), the dynamic topography is then

$$z_{BC} = ssh - z_g - z_{BT} - z_e. \tag{A3}$$

The geoid z_g' obtained by Carnes (private communication) is used as z_g. A geoid has been estimated by Glenn et al. (1991) using a similar technique. The Carnes et al. geoid is computed as follows: Since z_g is constant in time, at least on the time scales considered here, it may be estimated by subtracting a 1-year mean dynamic height anomaly, $\bar{z}_{BC}$, from the mean sea surface height $\overline{ssh}$ for the same period.

$$z_g' = \overline{ssh} - \bar{z}_{BC}. \tag{4}$$

The approximations used to obtain Fq. (4) are discussed by Maul et al. (1988). The first step in estimating $\bar{z}_{BC}$ is to use a water-mass-cased climatology and feature models to construct a three-dimensional thermal analysis of the Gulf Stream region for each map in a year-long series of weekly, NAVOCEANO-prepared front and eddy maps. The dynamic height anomaly was then estimated for each thermal analysis and the ensemble of dynamic height anomaly fields subsequently averaged. The $\overline{ssh}$ is obtained by making an orbit error correction to each track of sea level data and averaging the ensemble of ssh's. If the track length is much less than the length of an orbit, e.g., 1000 km, then the orbit error can be removed by making a linear correction. (This geoid is determined only along the tracks of altimetry data and is not a two-dimensional field.)

Maul et al. (1988) have proposed using in situ inverted echo sounder/pressure gauge and/or island tide gauge data to eliminate the orbit error in the dynamic topography along the track. These

data would provide an estimate of the dynamic topography along the track. By differencing the uncorrected altimeter-derived estimate and the in situ estimate, the orbit error can be explicitly estimated and, hence, corrected.

The technique used here to correct for orbit error, which was developed independently, has similarities with that of Maul et al. (1988) and also Carnes et al. (in preparation) but differs in several respects. In this technique, a reference dynamic height anomaly profile is constructed along the ground track. The purpose of this construction is to build a quasi-realistic profile that has a sharp gradient at the location of the instantaneous front and resembles climatology elsewhere. This series is a reasonable first guess of actual dynamic height anomaly. The difference between the reference dynamic topography and the first estimate is then an estimate of the orbit error. A linear correction in bias ζ and tilt γ is applied to z such that a least-squares linear fit of z agrees with that of the reference series. The distance along the track is x. As a result of this correction, the bias and tilt of the corrected z is the same as that of the quasi-realistic estimate. Admittedly, this technique cannot account for large-scale fluctuations in the sea surface topography due to large-scale changes in the oceanography. The dynamic topography is then

$$z_{BC} = ssh - z'_g - z_{BT} - z_e - (\zeta + \gamma x).$$ (5)

In practice, the baratropic term z_{BT} is neglected.

Figure A1 shows the method of construction. The solid line in Fig. A1 is the 1-year mean dynamic height anomaly obtained by Carnes et al. (in preparation), which has a broad gradient associated with the meandering of the sharp Gulf Stream front. This mean dynamic height anomaly is modified by inserting into the series a sharp linear gradient in the dynamic height anomaly at the
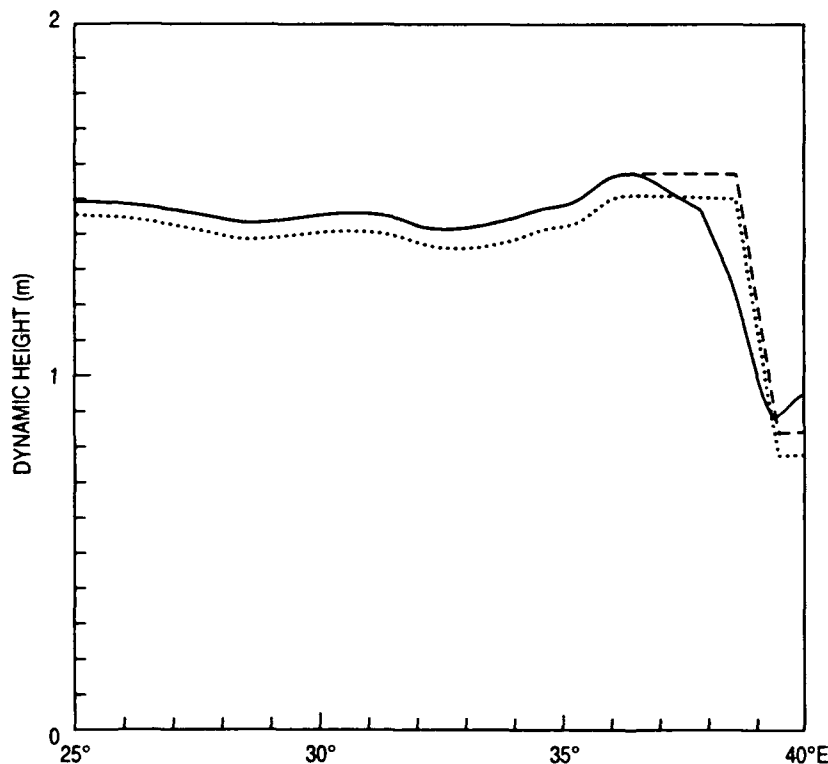

Fig. A1 — The reference dynamic topography constructed for use in the orbit error correction. The curves shown are the 1-yr mean dynamic height anomaly (solid curve), the mean dynamic height anomaly with a linear front inserted at the location of the instantaneous front (long dash curve), and the mean dynamic height anomaly with the constructed front and a steric correction (short dash curve).

observed instantaneous location of the Gulf Stream front (see the long dashed line of Fig. A1). To eliminate the climatological gradient in the dynamic height anomaly in the vicinity of the front, the dynamic height anomaly between the instantaneous front and the climatological maximum south of the front is made a constant (see Fig. A1). A constant value of 0.85 m is assumed north of the front. Next, a steric correction to the dynamic height anomaly is made (see the short dashed line in Fig. A1). The magnitude of the steric correction is determined by interpolating in time the magnitude of the monthly mean steric change for Sargasso and Slope waters. The correction is applied separately to the Sargasso and Slope waters. Rings are not considered in this implementation but could be readily incorporated into the algorithm.